ADVANCES IN MATERIALS SCIENCE, Vol. 22, No. 2 (72), June 2022

DOI: 10.2478/adms-2022-0008

Ubong Williams Robert[1], Sunday Edet Etuk[2], Sylvester Andrew Ekong[1], Okechukwu Ebuka Agbasi*[3], Nsikak Edet Ekpenyong[1], Samuel Sunday Akpan[1], Eme Aniefiok Umana[4]

[1]Department of Physics, Akwa Ibom State University, Ikot Akpaden, Mkpat Enin, Akwa Ibom State, Nigeria
[2]Department of Physics, University of Uyo, Uyo, Akwa Ibom State, Nigeria
[3]Department of Physics, Michael Okpara University of Agriculture, Umudike, Abia, Nigeria
[4]Department of Chemistry, Akwa Ibom State University, Ikot Akpaden, Mkpat Enin, Akwa Ibom State, Nigeria

**agbasi.okechukwu@gmail.com*

ELECTRICAL CHARACTERISTICS OF DRY CEMENT – BASED COMPOSITES MODIFIED WITH COCONUT HUSK ASH NANOMATERIAL

ABSTRACT

Coconut husk is generated yearly as waste in large quantities but majorly under-utilized. Also, as a result of high embodied carbon, cement production is one of the largest contributors to construction sector carbon footprint. Since accumulation of unmanaged agro-waste like coconut husk has an increased environmental concern due to its pollution effect, recycling it into sustainable construction materials is a viable solution for future generation. In this study, experiments were performed to investigate the influence of coconut husk ash nanomaterial (CHAN) inclusion on electrical characteristics of plain cement paste (BCP) and mortar (CSM) samples at curing ages of 7 and 28 days. The results showed increase in electrical resistivity, thermal constant, and activation energy with curing duration for heating and cooling cycles of BCP and CSM. With inclusion of CHAN, the developed cement paste (CAP) and mortar (CASM) possessed lower values in all cases compared to their counterparts. Also, during heating at 28 days, both the CAP and CASM exhibited decrease in thermal constant. Though electrical resistance of all the samples varied inversely with temperature, CAP and CASM were found to possess greater potentials to make building structures intrinsically smart. Hence, in addition to solving disposal problems, utilization of coconut husks as described herein could enhance development of safe, inexpensive, and sustainable buildings that have large temperature sensing volume.

Keywords: *Activation energy; building; electrical resistivity; temperature sensing; thermal constant*

INTRODUCTION

Cement is a powdery substance popularly utilized as a binder and an extremely important constituent of materials such as concrete, sandcrete blocks, grout (paste), and mortar which are extensively used for construction of buildings (houses). Production of cement causes increase in carbon dioxide emission profile and absolute reliance on its use leads to rising and prohibitive costs of procurement. On the global scale, building and construction are held accountable for 39% of the energy-related carbon emission [1] which the construction industry is responsible for 23% of the total carbon dioxide released in economic activities [2].

The data gathered and reported by Andrew [3] revealed that the global process emission from cement production between 1928 and 2018 reached 1.50 ± 0.12 Gt of carbon dioxide. All these point to the fact that cement production is one of the largest contributors to the construction sector carbon footprint due to its high embodied carbon. Therefore, the consistent increase in the production of cement needed to be checked in order to handle the situation effectively.

Observably, one major achievement of nanotechnology has been the successful introduction of nanomaterials into cement. This reduces clinker production which in turn lowers the energy demand and gives cement –based products that have improved properties. For instance, incorporation of nano-TiO_2 [4, 5], nano-SiO_2 [6], and nano-Al_2O_3 [7] in cementitious materials can increase cement hydration rates, enhance durability properties, improve the pore structure, flexural strength and compressive strength of the resulting composites. Not only that, addition of carbon nanotubes can effectively improve the strain sensing capability of cement-based composites, proving them to act as piezoresistive sensors [8, 9]. According to Cadavid-Giraldo et al [10], transition from conventional materials to low-carbon and energy-efficient materials for construction is a preferable method to mitigate the carbon dioxide emission and the climate change crisis. In this regard, previous studies [11, 12] have revealed that utilization of fly ash and slag as supplementary cementitious materials (SCMs) is a practical possibility as they can bring down the embodied carbon associated with cement production by 10 – 20%. However, slag production is less than 10% of cement production and coal-based electricity production (for generation of fly ash) is not a sustainable process, thus signifying that the long-term availability of such limited but widely used industrial by-products is doubtful.

That being the case, there is no doubt that incorporation of solid plant-based agro-waste ashes into cement is a sustainable option. This is because agro-wastes are usually generated in large quantities. Thus, such practice enhances the reuse of the residual ashes instead of disposal as a waste which can cause severe pollution and it is a viable valorization route which can reduce the need for cement and associated footprint of carbon. Recently, Charitha et al [13] reviewed several studies carried out on the use of agro-waste ashes in cementitious systems. They reported that sugarcane bagasse ash, sugarcane straw ash, palm oil fuel ash, rice husk ash, and elephant grass ash can be used as alternative SCMs up to 20% whereas rice straw ash, wheat straw ash, corn cob ash, groundnut husk ash, wood ash, bamboo leaf ash, coconut shell ash, and tobacco ash can be blended up to 10% as optimum cement replacement level. The said report showed improvements in all the investigated properties some of which were mechanical properties (tensile strength, flexural strength, compressive strength), durability properties (water absorption, sorptivity, porosity, chloride attack, sulphate attack, chloride penetration, permeability, drying shrinkage), and microstructures of cement – based systems.

It has been observed that though coconut husk is a promising material for production of composite ceilings and other insulation panels [14-17], it is majorly under-utilized. As of April 29, 2019, it was reported in the Guardian Newspaper that increase in global demand for coconut exceeded 500% in the past five years. Also, Zafar [18] noted that coconuts are produced in 92 countries worldwide on more than 10 million hectares and each fruit is made up of 40% husk. This was as Tajuddin et al [19] had observed that approximately 15 to 20 million tons of coconut husk are generated yearly, making it abundant as a cheap residue from coconut production. In this study, attempts are made to explore a safe way to manage such dignified agro-waste and also make its economic value known for the purpose of creating endless sustainable construction opportunities. Specifically, this study is designed to focus on how incorporation of coconut husk ash nanomaterial as partial cement substitute can affect the electrical characteristics of cement-based systems such as pastes and mortars,

particularly, in relation to temperature variations. It is well established that electrical parameters are useful for the study of behavior of cement-based systems [20 – 23]. Since affordable and sustainable buildings must be safe as well, temperature monitoring is a necessity and electrical properties are very relevant to the use of structural materials for non-structural purpose. By so doing, accurate prediction of temperature effects on performance, operations, and safety of structures can be ensured. To the best of the authors' knowledge, there is no report made in the direction of this work in the literature. As such, it is hoped that findings from it will be greatly beneficial to engineers, builders, researchers, waste managers, and can also lead to technological progress in housing sector and construction industry.

EXPERIMENTAL CONSIDERATION

Materials description and acquisition

Portland Limestone Cement (CEM II – BL 32.5R), fine aggregate (river-bed sand), coconut husks, and potable water (from borehole) were the major precursors utilized in this study. The sand was clean and free from deleterious substances. Whereas the husks were gathered as discarded waste materials from local coconut growers, the cement and sand were collected from a building construction site. These materials were sourced within Uyo Local Government Area, Akwa Ibom State, Nigeria.

Processing and analysis of the materials

The husks were submerged in water at 26^{o}C in order to remove dirts and other accompanying impurities from them. After 20 minutes, they were removed from the water, sun-dried to constant weight and then burnt in controlled environment inside furnace at 700^{o}C to produce ash. The coconut husk ash produced was milled into nanomaterial by means of high-energy ball miller ($E_{max,}$ manufactured by RETSCH GmbH) operated at 500 rpm for 5 hours. This machine is capable of reducing material feed from about 5mm particle size to as fine as less than 80 nm. The sand collected was also dried completely in air and then after subjected to gradation test by sieving method [24]. Angle of repose, loose bulk density, and specific gravity of the sand, cement, and coconut husk ash nanomaterial (CHAN) were determined as detailed elsewhere [25] for five trials each. Chemical composition analysis of the CHAN was performed [26] after which that of 4:1 cement – CHAN mixture was computed. The choice of 20% cement replacement with the CHAN to form the said mixture was based on the fact that such proportion is mostly the optimum level for pronounced effect of agro-waste ashes on the properties of cement-based composites as noted by many researchers including [13, 27]. In addition, morphological characterization of the ash materials was performed with the aid of Scanning Electron Microscope (Philips XL – 30) and XRD analysis was carried out on the CHAN using X-ray diffractometer (Schimadza XRD-60).

Mix design and samples preparation

Two types of cement-based composites, namely paste and mortar, were prepared according to the mix design shown in Table 1. Batching of the mixture constituents was by weight method. Each mixture was cast in separate Plexiglas molds of cross-section 52 mm x 26 mm and height 14 mm.

Table 1. *Research mix design used in this study*

Composite constituents	Ratio of the proportioned mix constituents Cement: CHAN: Sand	Sample code	Number of samples	Cement to sand ratio (constant)	Water–cement ratio (constant)
Cement	1:0:0	BCP	10	1:5	0.8
Cement and CHAN	4:1:0	CAP	10		
Cement and sand	1:0:5	CSM	10		
Cement, sand, and CHAN	4:1:25	CASM	10		

Two copper plates (each with a width of 20 mm and a height of 35 mm) were embedded into the mixture immediately after casting and compaction. The embedment length and interval between the plates were 13 mm and 30 mm respectively. These copper plates served as electrodes and care was taken to ensure that they were at same distances from the ends of the sample. All the samples were similarly prepared and they were demolded after 24 hours before being cured in a shade by sprinkling water on them twice daily. Out of the ten samples prepared in each case, five were cured for 7 days while the remaining ones were cured for 28 days. These curing ages are frequently adopted in the literature for masonry units.

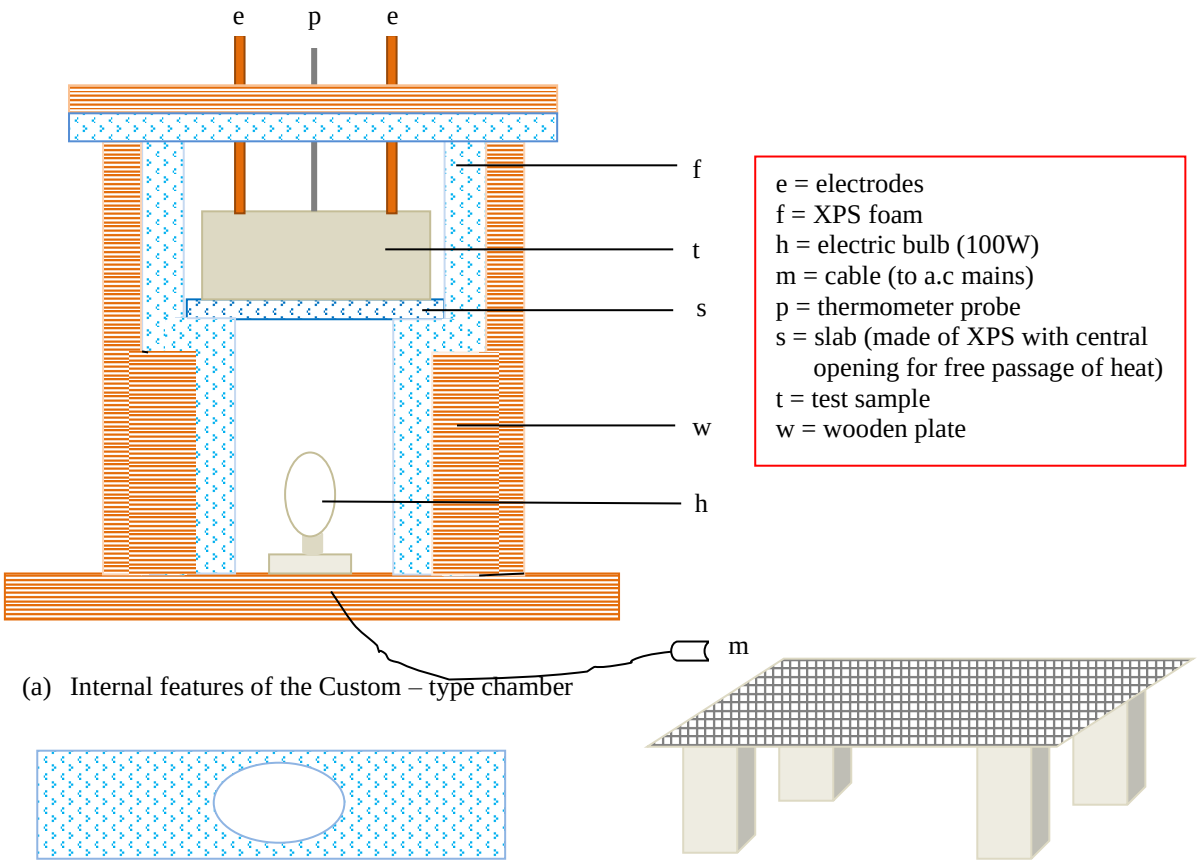
At the end of curing, the samples were subjected to continuous sun-drying and weighing for several weeks until no change in their weights was obtained and they were thus regarded as being completely-dry. Sun-drying of the samples was preferred to oven-drying because the latter process is usually performed at a standard temperature of 105^{o}C for 24 hours and that can cause cement paste to exhibit some damage at that temperature. The electrical characteristics of the dried samples were examined. Keeping in mind that each mixture was prepared with water, constituents were batched by weight (mass), and volume is the ratio of mass to density, aggregate (sand) volume fraction, V_{af} was calculated as

$$V_{af} = \frac{V_a}{V_T} \tag{1}$$

where V_a = volume of aggregate in the mixture, and V_T = combined volume of all the mixture constituents

Test set-up features

Figure1 shows the features of the custom - made set-up used in this work for heating and cooling of each sample. Four wooden plates (cut from Medium-density-fiber sheet) each measuring 250 mm in height and 15 mm in thickness were used to form the exterior of which each surface measured 190 mm in width. From the top of the chamber, the plates were countersunk internally to a depth of 50 mm with thickness of 10 mm after which their inner surfaces were carefully covered with extruded polystyrene foam (XPS) of thickness 30 mm (having thermal conductivity of 0.033 $Wm^{-1}K^{-1}$ at 24^{o}C) in order to significantly reduce heat exchange with the surroundings during heating schedule. The countersunk base served as a support for a slab (of dimensions 116 mm x 116 mm x 30 mm) made from the XPS. This slab was prepared with a central hole (of diameter 25 mm) for free passage of heat to a test sample. The lid of the chamber was also made from the XPS, sliced to a thickness of 10 mm with length and width being 190 mm and 100 mm respectively. Pilot holes were provided in the lid for accommodation of thermometer probe and sample electrodes. The heat source was a 100W incandescent bulb fixed in a holder mounted on a wooden plate (with a provision for the flow of current from a.c mains through a 1.5mm electric cable into the bulb). This plate measured 230 mm x 230 mm x 15 mm and it served as the base of the system.



(a) Internal features of the Custom – type chamber

(b) Top view of the slab

(c) Wire net (placed on concrete stands)

Fig. 1. Schematic illustrations of the system components for heating and cooling schedules

Measurement procedure and properties determination

The samples were stored in a laboratory under a controlled temperature of 18 ± 1°C for 24 hours. Then after, a sample was placed on the slab before the chamber was covered. The entire system was kept on its base, ensuring that it housed the bulb properly. A digital thermometer (Model No 308) was calibrated and equipped with type – K probe which was inserted through the lid of the chamber to contact the top of the sample. This probe was clamped to ensure that it remained in its position throughout the measurement durations. Also, an LCR meter (Model 9183, Lutron) was calibrated and its probes were connected to the electrodes of the sample under test (LCR stands for Inductance-Capacitance-Resistance). By enabling electric current to flow through the bulb filament, heat was generated within the chamber and under the sample. Progressive changes in the temperature and electrical resistance of the sample were observed on the thermometer and LCR meter, respectively, as the heat (radiated from the bulb) passed through the slab opening and was absorbed by the sample. Heating was made to proceed intermittently and the electrical resistance – temperature data were obtained at 5°C intervals from 20°C. Immediately when the readings at 50°C were taken, the system was removed from its base and then kept on the wire net placed on concrete stands so as to allow for steady cooling as air from the surroundings penetrated the unit from its bottom. Like in the case of the heating schedule, electrical resistance – temperature data of the samples were also obtained for the cooling cycle. For each type of composite, the mean of the electrical resistance values obtained for the replicates was computed per temperature, T both for heating and cooling cycles. Using the data obtained, the electrical resistivity, ρ was calculated based on the relation

$$\rho = \frac{RA}{L} \tag{2}$$

where R = mean electrical resistance value, A = cross-sectional area of the sample surface in contact with the electrodes, and L = separation of the electrodes.

Also, a graph of R against T was plotted to appraise the nature of existing relationship between them. Further, from the plot of $ln\,R$ against $1/T$ (where T is in Kelvin), thermal constant, β was deduced according to the relation [28]

$$R = R_o \exp\left(\frac{\beta}{T}\right) \quad (3)$$

where R_o = electrical resistance at infinity (reference electrical resistance) with which the temperature coefficient of resistance, α was obtained thus

$$\alpha = \pm \left(\frac{\beta}{T^2}\right) 100\% \quad (4)$$

considering the fact that the negative sign is necessary only if R and T vary inversely. The corresponding activation energy, E_a was determined from the relation

$$\beta = \frac{E_a}{k} \quad (5)$$

where k= Boltzmann's constant.

RESULTS AND DISCUSSION

Table 2 shows the index characteristics of the cement, CHAN, and sand utilized in this study. It can be inferred from the results that sand is the heaviest among the materials, followed by cement and then the CHAN. The static angle of repose of the cement is 16.7% greater than that of the sand but 0.5% less compared to the value obtained for the CHAN. Based on the fact that angle of repose is inversely proportional to the particle size of a material [29, 30], it implies that the sand particles are the largest in size whereas those of the CHAN are the smallest. However, since angle of repose of 36º to 40º indicates a fair flow property [31], it can be adjudged that the cement, CHAN, and sand possess acceptable characteristics for use as in this case. Figure 2 reveals that the sand contains assorted particle sizes and hence, it is well graded for use.

Table 2. *Characteristics of the materials used*

Parameters	Mean value per material		
	Cement	CHAN	Sand
Loose bulk density (kgm^{-3})	1250.0	342.5	1569.9
Specific gravity	3.15	2.50	2.75
Static angle of repose (º)	39.8	40.0	34.1

In terms of chemical composition (Table 3), the most abundant oxide in the cement is CaO and then SiO_2 before Al_2O_3. A similar trend occurs in the case of cement – CHAN mixture whereas SiO_2 is the most prominent in the CHAN. The loss on ignition is greater for CHAN compared to the cement. This could be attributed to high content of carbon-based component in the CHAN. By considering the stipulations that a good quality cement must contain 60 – 67% of CaO, have silica ratio (that is, the ratio of SiO_2 content to the combined proportion of Al_2O_3 and Fe_2O_3) between 1.7 and 3.5, and exhibit maximum of 12% loss on ignition [32], the cement type utilized in this study can be regarded to be of recommended quality. Also, since the fractions of SiO_2, Al_2O_3, and Fe_2O_3 in the CHAN sum up to a value that is even greater than 70% required as minimum proportion for pozzolans, it can be posited that CHAN is a pozzolanic material in this case. The XRD patterns and SEM images shown in Figure 3 give further insights on the ash materials. The micrograph of the as-prepared ash

shows that the particles are structurally pentagonal with sizes ranging about 1-3μm (before being converted into nano-size). These particles have a very well defined texture with heterogeneous surface channels. The monograph of the CHAN reveals that the particles have been reduced to far less than 80 nm. Also, it can be seen from the diffractograms that some major and minor peaks are recorded for the oxide crystals in the ash.

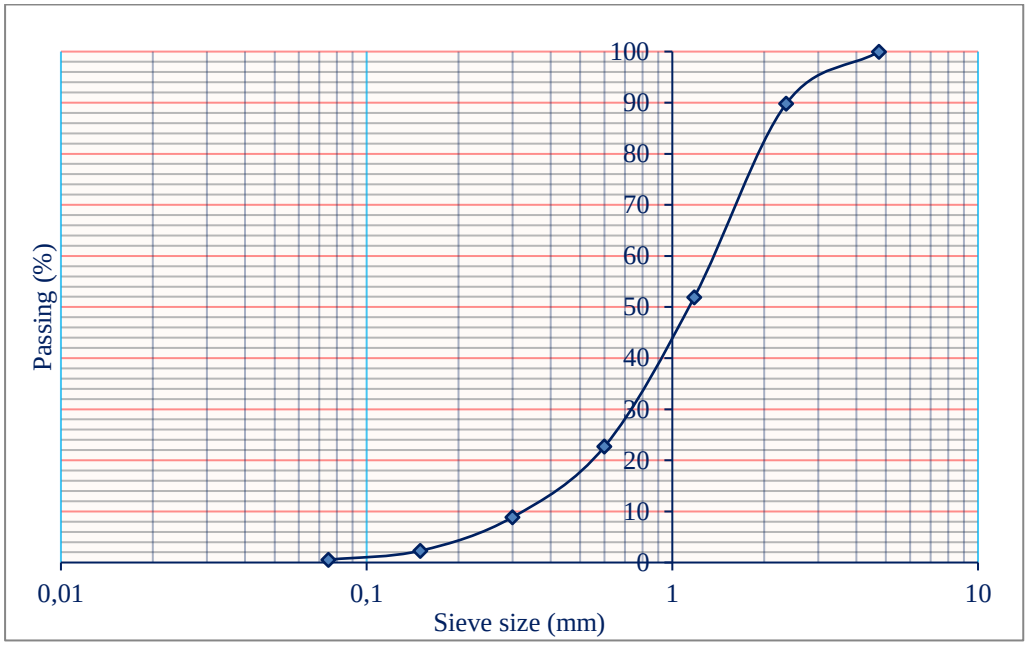
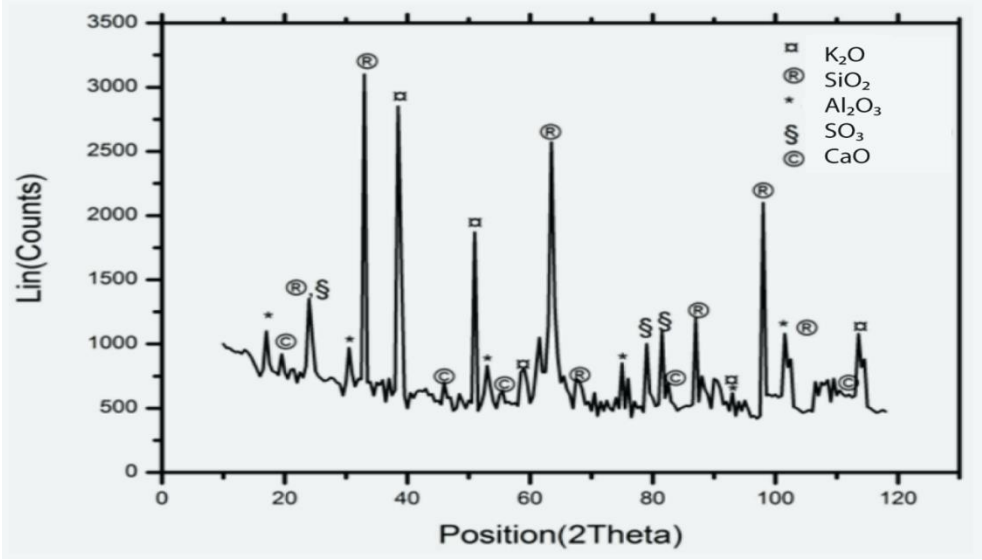


Fig. 2. Grading curve of the sand used

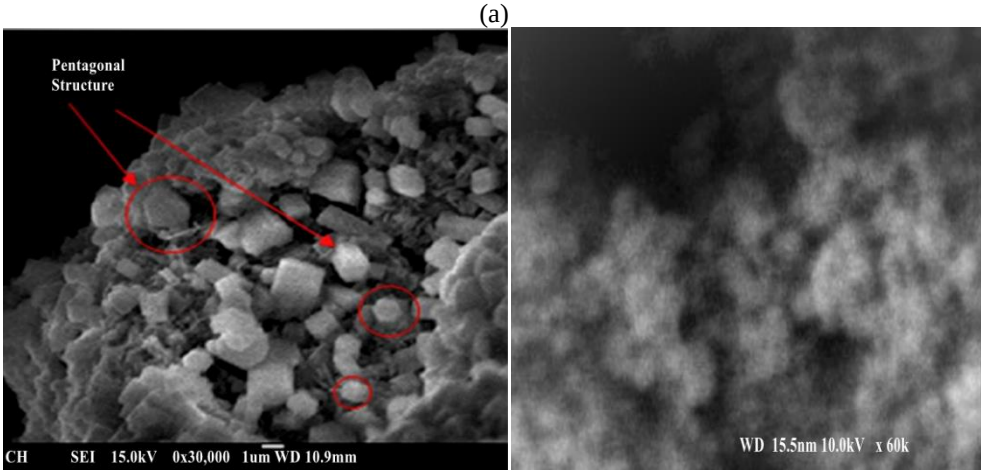
Table 3. *Some oxides composition of the cement, CHAN, and cement – CHAN*

Oxide contents		Proportion (wt %)		
Name	Formula	Cement	CHAN	Cement - CHAN
Silicon oxide (Silica)	SiO_2	17.82	71.93	28.64
Aluminium oxide (Alumina)	Al_2O_3	3.29	0.84	2.80
Ferric oxide	Fe_2O_3	2.55	0.21	2.08
Potassium oxide	K_2O	0.28	4.77	1.18
Calcium oxide (Lime)	CaO	60.78	0.30	48.68
Sulphur trioxide	SO_3	2.52	3.45	2.71
Loss on ignition	LOI	1.40	9.32	2.98

It is noteworthy that temperature is a weather condition and it is capable of affecting construction materials. For instance, abrupt temperature changes can cause cracking and spalling due to thermal shock. Also, aggregate expansion can bring about distress within cement-based materials.



(a)



(b)

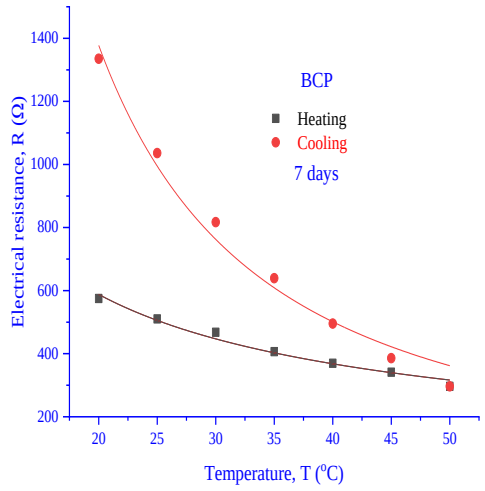
Fig. 3. (a) RXD diffractograms of the CHAN, (b) SEM images of the ash materials

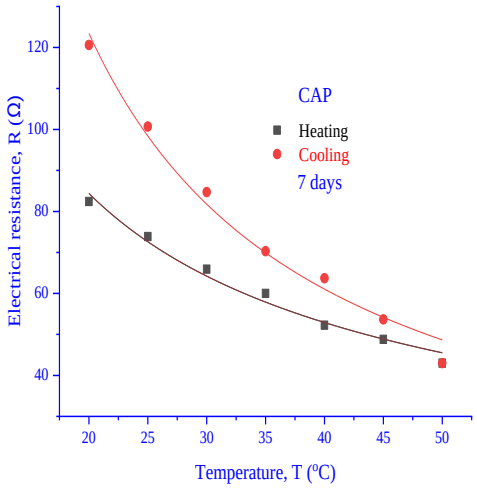
From Table 4, it is observed that though cooling process yields greater values than in the case of heating, the electrical resistance of each sample decreases with increasing temperature irrespective of the curing age. This means that as temperature rises, the samples become more electrically-conductive. Figure 4 illustrates that the resistance – temperature relationship is an exponential decay, typical of a negative temperature coefficient (NTC) thermistor. The observed tendency is due to the activation energy associated with the electron jumping across interfaces in the samples. This phenomenon could be utilized for temperature monitoring since temperature in itself is nothing more than a quantification of heat energy. Meanwhile, temperature monitoring in buildings is conventionally performed by means of embedded/attached sensors. Aside being costly, such devices have sensing ability that is location-specific. Consequently, they do not enhance accurate prediction of temperature effects on performance, operation, and safety of structures. On the contrary, the cement pastes and mortars studied in this work can be used for plastering purpose to cover rough walls and uneven surfaces in the construction of houses as well as other structures. Thus, with their self-sensing ability, advantages in terms of low cost, high durability, large sensing volume, and absence of mechanical property loss can be enjoyed as the resulting smart structure responds to temperature changes in a desirable fashion. In all of these, samples with CHAN content show improved tendency over their counterparts.

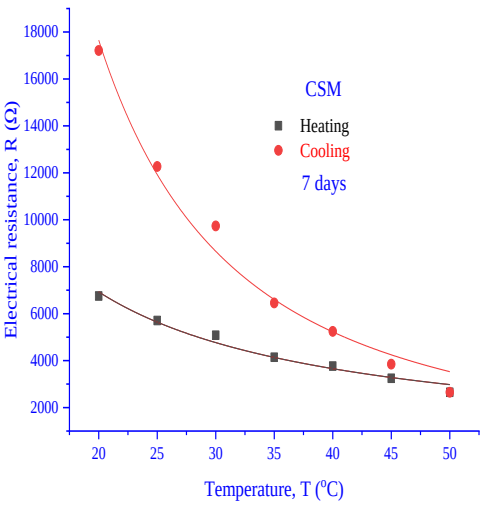
Table 4. *Electrical resistance – temperature regime data*

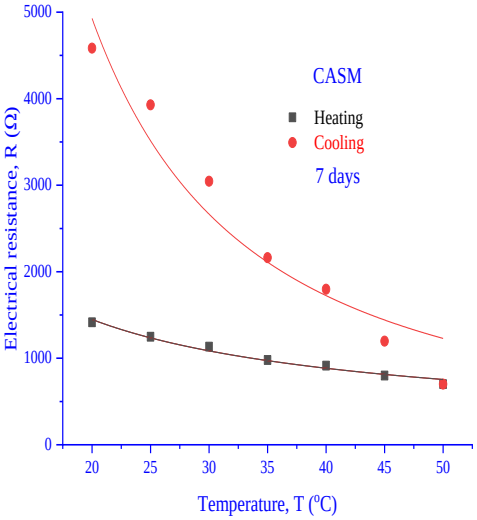
Age of curing	Temperature, T (°C)	Mean values of electrical resistance, R (Ω)			
		BCP	CAP	CSM	CASM
7 days	20.0	5.750E2 (1.335E3)	8.241E1 (1.206E2)	6.753E3 (17.214E3)	1.415E3 (4.584E3)
	25.0	5.102E2 (1.036E3)	7.387E1 (1.007E2)	5.709E3 (12.272E3)	1.248E3 (3.928E3)
	30.0	4.679E2 (8.169E2)	6.592E1 (8.472E1)	5.082E3 (9.736E3)	1.134E3 (3.045E3)
	35.0	4.063E2 (6.393E2)	6.000E1 (7.031E1)	4.143E3 (6.456E3)	9.800E2 (2.162E3)
	40.0	3.695E2 (4.954E2)	5.224E1 (6.372E1)	3.765E3 (5.246E3)	9.148E2 (1.798E3)
	45.0	3.414E2 (3.859E2)	4.880E1 (5.367E1)	3.248E3 (3.849E3)	7.989E2 (1.197E3)
	50.0	2.963E2 (2.963E2)	4.300E1 (4.300E1)	2.653E3 (2.653E3)	7.000E2 (7.000E2)
28 days	20.0	3.610E3 (6.569E3)	3.456E2 (6.480E2)	59.590E3 (80.508E3)	4.582E3 (13.743E3)
	25.0	3.059E3 (5.057E3)	3.095E2 (5.175E2)	44.714E3 (57.239E3)	4.087E3 10.287E3)
	30.0	2.688E3 (4.023E3)	2.853E2 (4.428E2)	35.889E3 (45.267E3)	3.768E3 (8.553E3)
	35.0	2.232E3 (3.075E3)	2.510E2 (3.373E2)	25.890E3 (29.880E3)	3.290E3 (5.929E3)
	40.0	1.989E3 (2.440E3)	2.336E2 (2.974E2)	20.980E3 (23.392E3)	3.039E3 (4.676E3)
	45.0	1.714E3 (1.900E3)	2.114E2 (2.433E2)	17.896E3 (18.811E3)	2.785E3 (3.754E3)
	50.0	1.443E3 (1.443E3)	1.861E2 (1.861E2)	12.152E3 (12.152E3)	2.419E3 (2.419E3)

Values in parenthesis are from measurements taken during cooling schedule









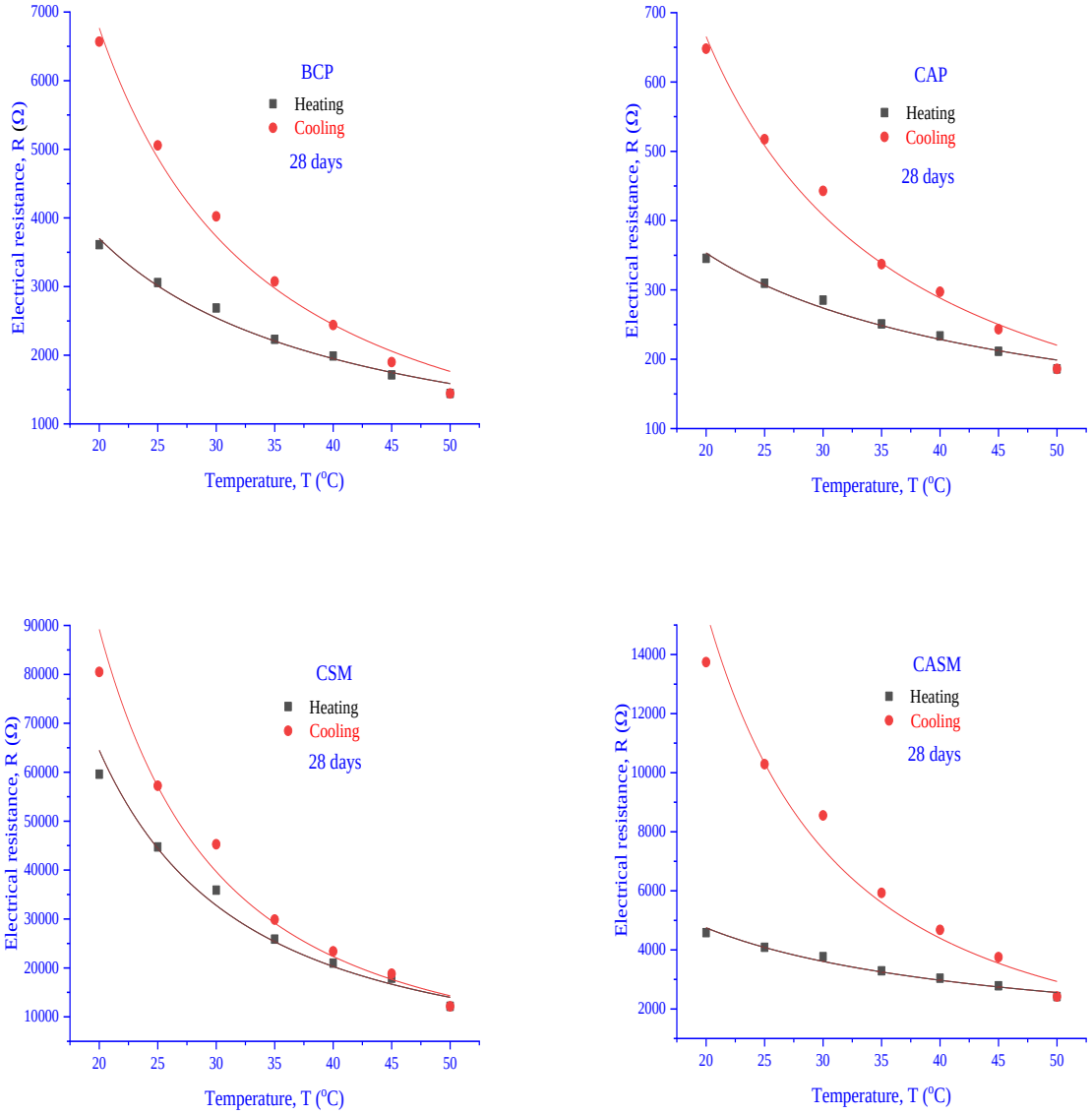


Fig. 4. Electrical resistance – temperature relationships of the samples at curing ages of 7 days and 28 days

In Table 5, the summary of the investigated properties is presented. For the heating and cooling cycles per curing age, CAP has lower electrical resistivity compared to BCP as a result of inclusion of CHAN. This, plausibly, is because the pozzolanic activity of CHAN produces an extra amount of calcium silicate hydrate along with a reduced amount of calcium hydroxide. In turn, this lowers the average pore volume in CAP in comparison with that of BCP. According to Ternero et al [33], pores have a marked influence on the passage of an electric current. Usually, diffuse interface exists in pastes and in this case, the fineness of CHAN particles enhances inter-packing behavior thereby minimizing pore sizes in CAP. Interestingly, it could be argued that since CHAN is inherently more electrically conductive than the cement matrix, it is possible for its inclusion to lower the resistivity values for CAP with respect to the values obtained for BCP. In the cases of mortars (CSM and CASM), electrical conductivity represents a compromise between two important factors, namely, the insulating effect of the aggregate (sand) and the development of transition zone between the aggregate volume fractions. At the age of 7 days, the resistivity of CSM is 91.44% (for

heating cycle) and 93.94% (for cooling cycle) greater than the values obtained for BCP. Also, at the age of 28 days, the increments are found to be 92.24% and 91.85% respectively. Though the values obtained for CASM are lower than those recorded for CSM, they are greater when compared to the resistivity values of BCP and CAP. This shows that the insulating effect of the aggregate dominates and raises electrical resistivity of the mortar samples. The lower values of resistivity obtained for CASM compared to the CSM is due to the inherent conducting ability of CHAN as noted earlier in this study. This observation on CSM and CASM is in line with the findings reported by Tumidajski [34] that when volume fraction of aggregate is greater than 0.1, the electrical conductivity of mortar decreases. Observably, CSM and CASM have aggregate volume fraction of 0.653 and 0.604 respectively thereby exhibiting increase in electrical resistivity over BCP and CAP. Presumably, thermal degradation causes the resistivity values of the samples to be higher during cooling than during the initial heating.

Table 5. *Computed values of the investigated properties*

Sample code	V_{af} (10^{-2})	7 days				28 days			
		$\rho\ (\Omega m)$	$\beta\ (K)$	$E_a\ (eV)$	$\alpha\ (\%/K)$	$\rho\ (\Omega m)$	$\beta\ (K)$	$E_a\ (eV)$	$\alpha\ (\%/K)$
BCP	0.0	6.98 (16.20)	2051 (4732)	0.179 (0.408)	- 2.39 (- 5.51)	43.80 (79.70)	2851 (4742)	0.246 (0.409)	- 3.32 (- 5.52)
CAP	0.0	1.00 (1.46)	2040 3138)	0.176 (0.270)	- 2.37 (- 3.65)	4.19 (7.86)	1865 (3824)	0.161 (0.330)	- 2.17 (- 4.45)
CSM	65.3	81.94 (208.86)	2863 (5784)	0.247 (0.498)	- 3.33 (- 6.73)	723.03 (977.32)	4833 (5795)	0.416 (0.499)	- 5.62 (- 6.74)
CASM	60.4	17.17 (67.75)	2178 (5754)	0.188 (0.496)	- 2.53 (- 6.70)	55.59 (166.75)	1963 (5293)	0.169 (0.456)	- 2.28 (- 6.16)

ρ = Electrical resistivity at 20°C
β = Thermal constant
E_a = Activation energy
α = Temperature coefficient of resistance
Values in parenthesis are based on cooling data

Thermal constant is related to the energies needed to form and move charge carriers that are responsible for electrical conduction. The trend in thermal constant (β- parameter) follows a similar pattern with respect to CHAN incorporation into the cement paste or mortar as the case may be. For heating cycles at the age of 7 days, reduction by 0.54% is feasible in the case of CAP compared to the value obtained for BCP while the CASM has a value that is 23.93% less than the one obtained for the CSM. During cooling cycles, reductions are by 33.69% and 0.52% when comparing the thermal constant values obtained for the pastes and mortars respectively. At 28 days of curing, inclusion of CHAN causes the values to reduce by 34.58% during heating schedules and 19.36% during cooling schedules when the pastes (BCP and CAP) are compared. Also, the values for CASM are lower by 59.38% and 8.66% (during heating and cooling cycles respectively) compared to the ones obtained for CSM. These observations are indicative of the fact that inclusion of CHAN in plain cement paste or mortar leads to reduction in energy requirement for electrical conduction.

Activation energy reflects the energy for hopping of charge carrier in the composites and it describes the sensitivity for temperature sensing by a material. As expected, the activation energy decreases as thermal constant decreases due to inclusion of CHAN in the plain cement paste as well as mortar. This implies low energy requirement for sensing function as temperature varies. That is to say, CAP and CASM exhibit the tendency to sense temperature faster than BCP and CSM respectively. The negative temperature coefficient of resistance shown by the developed samples further portray that they could be used as NTC thermistors and temperature sensors.

CONCLUSIONS

The experiments performed in this study revealed that inclusion of coconut husk ash nanomaterial (CHAN) as partial cement substitute in either plain cement paste (BCP) or mortar (CSM) caused a marked influence on the electrical characteristics of the resulting paste (CAP) or mortar (CASM) respectively. Electrical resistivity, thermal constant, and activation energy values obtained at the age of 28 days for heating and cooling cycles were found to be greater than those recorded at 7 days for BCP and CSM. CAP and CASM possessed lower thermal constant values during heating schedule at 28 days. More so, the values of electrical parameters at both ages were found to be lower for CAP and CASM compared to those obtained for their counterparts (BCP and CSM respectively). Though all the samples exhibited negative temperature coefficient of resistance, it was observed that CAP and CASM have promising potentials for better temperature monitoring/sensing of building structures than BCP and CSM being the respective cement-based systems without the CHAN content. Hence, by utilizing coconut husks as described in this study, structures that can sense their own temperature without the need for embedded or attached sensors could be made.

REFERENCES

1. World Green Building Council, 2017. Global Status Report │UN environment and international energy agency [www Document]. URL. https://www.worldgbc.org/news-media/global-status-report-2017
2. Haung H., Gao X., Wang H., Ye H., 2017. Influence of rice husk on strength and permeability of ultra-high performance concrete, Construction and Building Materials. Vol. 149: 621 – 628,doi.org/10.1016/j.conbuildmat.2017.05.155
3. Andrew R.M., 2019. Global CO_2 emission from cement production, 1928 – 2018, Earth System Science Data, Vol. 11, Iss. 4: 1675 – 1710, doi.org/10.5194/essd-11-1675-2019
4. Sun J., Xu K.,Shi C., Ma J., Li W., Shen X., 2017. Influence of core/shell TiO_2@SiO_2 nanoparticles on cement hydration, Construction and Building Materials. Vol. 156; 114 – 122, doi.org/10.1016/j.conbuildmat.2019.08.124
5. Teixeira K.P., Rocha I.P., Carneiro L.D., Flores J., Dauer E.A., Ghahremaninezhad A., 2016. The effect of curing temperature on the properties of cement pastes modified with TiO_2 nanoparticles, Materials, Vol. 9, Iss. 11: 952 – 967, doi.org/10.3390/ma9110952
6. Khaloo A., Mobini M.H., Hosseini P., 2016. Influence of different types of nano-SiO_2 particles on properties of high-performance concrete, Construction and Building Materials. Vol. 113; 188 – 201,doi.org/10.1016/j.conbuildmat.2016.03.041
7. Liu J., Li Q., Xu S., 2015. Influence of nanoparticles on fluidity and mechanical properties of cement mortar. Construction and Building Materials. Vol. 101; 892 – 901,doi.org/10.1016/j.conbuildmat.2015.10.149
8. Pisello A.L., D'alessandro A., Sambuco S., Rallini M., Ubertini F., Asdrubali F., Materazzi A.L., Cotana F., 2017. Multipurpose experimental characterization of smart nanocomposite cement-based materials for thermal-energy efficiency and strain-sensing capability. Solar Energy Materials and Solar Cells, Vol. 161: 77 – 88,doi.org/10.1016/j.solmat.2016.11.030

9. Yoo D., You I., Lee S., 2017. Electrical properties of cement-based composites with carbon Nanotubes, Graphene, and Graphite Nanofibres. Sensors, Vol. 17, No. 5: 1064 – 1076,doi.org/10.3390/s17051064
10. Cadavid-Giraldo N., Velez-Gallego M.C., Restrepo-Boland A., 2020. Carbon emissions reduction and financial effects of a cap and tax system on an operating supply chain in the cement sector. Journal of Cleaner Production. Vol. 275: 122583, doi.org/10.1016/j.jclepro.2020.122583
11. Snellings R., 2016. Assessing, Understanding and Unlocking Supplementary Cementitious Materials, RILEM Technical Letters, Vol. 1: 50 – 55, doi.org/10.21809/rilemtechlett.2016.12
12. Serivener K., Martirena F., Bishnoi S., Maity S., 2018. Calcined Clay limestone cements (LC^3), Cement and Concrete Research. Vol. 114: 49 – 56,doi.org/10.1016/j.cemconres.2017.08.017
13. Charitha V., Athira V.S., Jittin V., Bahurudeen A., Nanthagopalan P., 2021. Use of different agro-waste ashes in concrete for effective upcycling of locally available resources. Construction and Building Materials. Vol. 285; 122851, doi.org/10.1016/j.conbuildmat.2021.122851
14. Robert U.W., Etuk S.E., Umoren G.P., Agbasi O.E., 2019. Assessment of Thermal and Mechanical Properties of Composite Board produced from Coconut (*Cocos nucifera*) Husks, Waste Newspapers, and Cassava Starch, International Journal of Thermophysics Vol. 40, No. 9: 83, doi.org/10.1007/s10765-019-2547-8
15. Bőger T., Bianchi S., Salzer C., Pichelin F., 2018.Binderless boards made of milled coconut husk: an analysis of the technical feasibility and process restraints. International Wood Products Journal, Vol. 9, No.1: 3– 8, doi.org/10.1080/20426445.2017.1400756
16. Panyakaew S., Fotios S., 2011. New Thermal Insulation boards made from coconut husk and bagasse, Energy and Buildings, Vol. 43, No. 7: 1732 – 1739, doi.org/10.1016/j.enbuild.2011.03.015
17. Glowacki B., Barbu M.C., Van Wijck J., Chaowana P., 2019. The use of coconut husk in high pressure laminate production, Journal of Tropical Forest Science, Vol. 24, No. 1: 27 – 36
18. Zafar S.,2021. Energy Potential of Coconut Biomass, Bioenergy Consult, Last accessed: March 19, 2021, www.bioenergyconsult.com
19. Tajuddin M., Ahmed Z., Ismail H., 2016. A review of natural fibers and processing operations for the production of binderless boards. BioResources, Vol. 11, No. 2: 5600 – 5617
20. Gui Q., Qin M., Li K., 2016. Gas permeability and electrical conductivity of structural concretes: Impact of pore structure and pore saturation, Cement and Concrete Research. Vol. 89: 109 – 119
21. Xiao L., Ren Z., Shi W., Wei X., 2016. Experimental Study on Chloride permeability in concrete by non-contact electrical resistivity measurement and RCM. Construction and Building Materials. Vol. 123: 27 – 34, doi.org/10.1016/j.conbuildmat.2016.06.110
22. Wang Y., Gong F., Ueda T., Zhang D., 2014. Theoretical Model for estimation of ice content of concrete by using electrical measurements. Procedia Engineering, Vol. 95: 366 – 375, doi.org/10.1016/j.proeng.2014.12.195
23. Gopalakrishnan R., Vignesh B., Jeyalakshmi R., 2020. Mechanical, electrical, and microstructural studies on mamo-TiO_2admixtured cement mortar cured with industrial waste water. Engineering Research Express. Vol. 2: 025010, doi.org/10.1088/2631-8695/ab899c
24. ASTM C136/136M, 2019. Standard Test Method for Sieve Analysis of Fine and Coarse Aggregates, ASTM International, West Conshohocken, PA
25. Robert U.W., Etuk S.E., Agbasi O.E., Okorie U.S., Abdulrazzaq Z.T.,Anonaba A.U., Ojo O.T., 2021. On the hygrothermal properties of sandcrete blocks produced with sawdust as partial replacement of sand. Journal of the Mechanical Behavior of Materials. Vol. 30, No. 1: 144 – 155, doi.org/10.1515/jmbm-2021-0015

26. Yahaya M.D., 2009. Physico-chemical classification of Nigerian cement. Australian Journal of Technology. Vol. 12, No. 3: 164 – 174

27. Okwadha G.D.O., 2016. Partial Replacement of Cement b Plant solid waste ash in concrete production. IOSR Journal of Mechanical and Civil Engineering. Vol. 13, No. 5: 35 – 40, doi.org/10.9790/1684-1305033540

28. Robert U.W., Etuk S.E., Agbasi O.E., Iboh U.A., Ekpo S.S., 2020.Temperature – dependent Electrical Characteristics of Disc-shaped Compacts fabricated using Calcined Eggshell Nanopowder and Dry Cassava Starch. Powder Metallurgy Progress. Vol. 20, Iss. 1: 12 – 20, doi.org/10.2478/pmp-2020-0002

29. Guiling X., Xiaoping C., Cai L., Pan X., Changsui Z., 2016. Experimental investigation on the flowability properties of cohesive carbonaceous powders, Journal of Particulate Science and Technology, 35(3); 322 – 329.doi.org/10.1080/02726351.2016.1154910

30. Lu H., Guo X., Liu Y., Gong X., 2015. Effects of particle size on flow mode and flow characteristics of pulverised coal, Kona Powder Part I., 32; 143 – 53.doi.org/10.14356/kona.2015002

31. USP, Powder Flow. In: The United States Pharmacopeia 30-National Formulary 25 Convention, Rockville, 2007.

32. ASTM C618, 2019. Standard Specification for Coal Fly Ash and Raw or Calcined Natural Pozzolan for use in concrete, ASTM International, West Conshohocken, PA

33. Ternero F., Rosa L.G., Urban P., Montes J.M., Cuevas F.G., 2021. Influence of Total porosity on the properties of sintered materials – A Review, Metals, Vol. 11, No. 5: 730, doi.org/10.3390/met11050730

34. Tumidajski P.J., 1996. Electrical conductivity of Portland Cement Mortars. Cement and Concrete Research. Vol. 26, No. 4: 529 - 534